# Synthesis of $YBa_2Cu_3O_{7-\delta}$ and $Y_2BaCuO_5$ nano-crystalline powders for YBCO superconductors using carbon nanotube templates

Yunhua Shi,*,† Tawfique Hasan,† Nadendla H. Babu,‡ Felice Torrisi,† Silvia Milana,† Andrea C. Ferrari,† and David A. Cardwell†

*Department of Engineering, University of Cambridge, Cambridge, CB2 1PZ, UK, and BCAST, Brunel University, Uxbridge, Middlesex, UB8 3PH, UK*

E-mail: ys206@cam.ac.uk

**Abstract**

We report the fabrication of nano-size superconducting $YBa_2Cu_3O_{7-\delta}$ (Y-123) and non-superconducting $Y_2BaCuO_5$ (Y-211) powders using carbon nanotubes as templates. Transmission electron microscopy shows that the mean particle size of Y-123 and Y-211 is 12 and 30nm, respectively. The superconducting transition temperature of the Y-123 nano-powder is 90.9K, similar to commercial, micron-scale powders fabricated by conventional processing. We also demonstrate improvements in the superconducting properties of YBCO single grain bulk samples fabricated using the nano-size Y-211 powder, both in terms of trapped field and critical current density. The trapped field reaches 553mT at 77K, with a$\sim$20% improvement compared to samples fabricated from commercial powders. This shows that our processing method is an effective source of pinning centres in single grain superconductors.

*To whom correspondence should be addressed
†Department of Engineering, University of Cambridge, Cambridge, CB2 1PZ, UK
‡BCAST, Brunel University, Uxbridge, Middlesex, UB8 3PH, UK

# Introduction

The superconducting properties of high temperature superconductors (HTS), such as Y-Ba-Cu-O (YBCO), depend strongly on their microstructure.[1] In particular, the critical current density, $J_c$, a key parameter for applications,[2] is proportional to the number of pinning centres per unit volume in the superconducting phase.[3] Non-superconducting phases with small dimensions (in the nm range) within the superconducting matrix form particularly effective flux pinning centres. These can generally be described as defects and non-superconducting second phases which 'pin' the quantized magnetic flux lines within the interior of a current carrying type II superconductor.[4] In particular, defects caused by neutron irradiation increase $J_c$ significantly.[5] The introduction of nano-structured secondary phases, such as $Y_2BaCuO_5$ (Y-211), $ZrO_2$[6] and $Y_2Ba_4CuMO_y$ (Y-2411(M)) (where M = Nb, W, Zr, Ag, Bi etc.) into the Y-123 superconducting phase has also long been the focus of bulk HTS research.[7–9] However, these secondary phases tend to form either inclusions, up to several microns in size, or agglomerates[10] during the high temperature process used to prepare the bulk material.[7,11–13] Thus, it is desirable to develop new methods to reduce the second-phase particle size, in order to improve flux pinning, hence $J_c$.

Bulk YBCO superconductors are commonly processed using the so-called Top Seeded Melt-Growth (TSMG) technique.[11,12] This involves mixing the Y-123 and Y-211 precursor powders in the required stoichiometric ratio, and then pressing them uniaxially to form pellets of the desired shape. A seed crystal is placed on top of this pellet, and the whole assembly is melt-processed to form a single grain.[11,12] The seed crystal promotes epitaxial heterogeneous nucleation and facilitates the growth from the melt.[11,12,14] In bulk YBCO, the resultant microstructure consists typically of Y-211 particles embedded in a single-crystal Y-123 matrix.[2,11,12] These Y-211 particles enhance magnetic flux pinning, which improves the current carrying capacity of the superconductor.[11,15] One of the key challenges for enhancing the magnetic flux pinning is to reduce the size of the Y-211 particles in the Y-123 matrix.[15] In the case of bulk HTS superconductors, the size of the particles which are mixed together and pressed to form the pellets is crucial in order to achieve high $J_c$. However, the mean particle size of commercially available powders is typically$\sim 1-3\mu$m.[16] This is a

consequence of their production by conventional solid-state reactions at elevated temperatures.[11,12] In order to fabricate a more homogeneous, finer powder, research has been carried out on improving the powder melting process, and combining this with ball milling,[17] or wet chemical synthesis of RE-123 or RE-211 precursors (where RE=Nd, Sm, Y).[9,18–20] For example, spray-drying 19 and co-precipitation[9] yield micro-structured (1-2 $\mu$m) Nd-123 and Y-123 powders with a homogeneous particle size distribution. Even better results may be achieved if the reaction is carried out in a confined environment.[18,20–22] For example, Ref. 20 used solution-based nano-emulsions to produce Y-211 powders with a particle size distribution between 30 and 100nm.

Carbon nanotubes (CNTs) can be used as templates for the fabrication of wires and tubes of various metals and metal-oxides[23] by filling or coating them with the desired material.[23–26] The aim of most previous work was to retain the shape/structure of the CNT templates.[23,26] Here we employ CNTs as template for nano-sized Y-211 and Y-123 powders, then used to fabricate bulk superconductors, but without the need to retain the CNT shape. We obtain Y-123 and Y-211 flake-like structures, rather than a solid, regular coating. These are then ground and calcined to produce nano-sized powders. Y-211 is chosen because it forms effective second phase flux pinning centres in YBCO.[15] We also make Y-123 powders using the same methodology to confirm that carbon is eliminated during the process. This is important because the superconducting transition temperature ($T_c$) of Y-123 is particularly sensitive to the presence of impurities.[27] Elimination of carbon is confirmed further by Raman spectroscopy. We fabricate YBCO nano-structured powders (Y-211 $\sim$30nm and Y-123 $\sim$12nm with a $T_c$ $\sim$90.9K) and a bulk sample using the nano-structured Y-211, with a$\sim$20% improvement in $J_c$ compared to that obtained from commercial micron-sized powders. Thus, our novel approach is a viable alternative to conventional powder processing.

# Results and Discussion

We use multi-wall CNTs (MWNTs) as they can be dispersed using low power sonication in water or other solvents, similar to single wall carbon nanotubes,[28,29] but offer a significantly cheaper

alternative as nano-structured templates. The MWNTs are purchased from Sigma-Aldrich.[30] The MWNT powder is sonicated and centrifuged as discussed in Methods. After the removal of unexfoliated bundles by centrifugation, the MWNT dispersions are mixed ultrasonically with a Y-123 nitrate aqueous solution. The resulting liquid mixture is then dried (Sample A). The corresponding Y-211-MWNT mixture is then prepared following the same approach (Sample B). The fully dried samples are calcined to eliminate nitrates and produce nano-structured powders, Samples A1 and B1. These are then ground further and calcined repeatedly until X-ray diffraction (XRD) confirms the formation of Y-123 (Sample A2) and Y-211 (Sample B2) phases. Note that repeated grinding and high temperature calcination, necessary steps for the fabrication of Y-123 and Y-211, significantly increase the particle size.[4,7,11,12] The $T_c$ of Sample A2 and commercially available Y-123 powder (99.9% purity, Toshima, Japan)[16] are then compared to assess the superconducting properties of Sample A2. The presence of even a small amount of carbon in the Y-123 lattice is known to reduce $T_c$ significantly.[31] For example, 0.5wt% carbon would cause $T_c$ to decrease by several degrees.[31] Raman spectroscopy of the precursors (A and B) and ground samples (A2 and B2) is used to monitor the presence of MWNTs or carbonaceous impurities. Raman spectroscopy is also used to confirm the formation of Y-123 and Y-211 phases in A2 and B2.

YBCO single grains are then fabricated from Sample B2 and commercially available Y-123 (Toshima) powder via TSMG.[11,12] In order to assess the superconducting properties of the samples derived with our new process, a single grain YBCO is also grown by TSMG using commercial Y-123 and Y-211 powders (See Methods for fabrication and characterization details).

Figure 1 shows a scanning electron microscope (SEM) image of Sample A1 after secondary calcination in air at 880 °C, but prior to grinding. No MWNTs can be seen, since they decompose into CO and $CO_2$ during calcination. The layered flake-like microstructure may be due to the formation of anisotropic tetragonal or orthorhombic Y-123 phases on the MWNT outer surface.

Unpolarized Raman spectra are acquired at 632.8nm excitation using a Renishaw InVia spectrometer, with a 100X objective. We use this wavelength to enhance detection of carbon species. Figure 2(a) compares the Raman spectra of the MWNT powder with the precursor salts/MWNTs

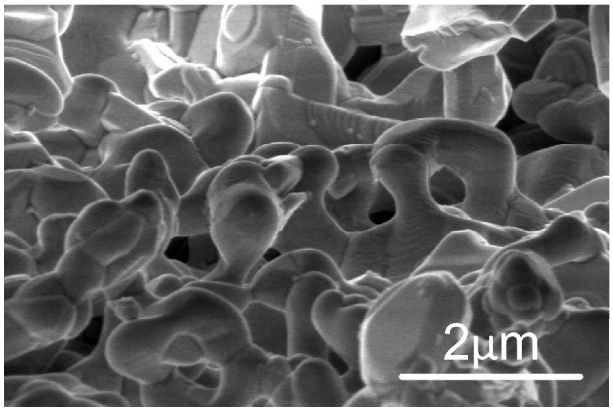


Figure 1: SEM photograph of powder A1 calcined at 880°C.

mixtures. The MWNT sample shows prominent D, G, 2D, D+D' and 2D' peaks, Figure 2(a). The G peak is present in any $sp^2$ carbon material and is due to the relative motion of carbon atoms, no matter if arranged in rings or chains.[32] Confinement and curvature split this band into $G^+$ and $G^-$ peaks in single-wall CNTs.[33] However such splitting is not observed in our sample, due to the large diameter of our nanotubes (having inner diameter of 5-10nm, outer diameter of 10-20nm).[30] The D peak is a 'breathing mode' of $sp^2$ bonded carbon atoms in six-fold rings and requires the presence of defects for its activation.[32] The relative intensity of the D to G peaks, I(D)/I(G), can be used to quantify the amount of disorder.[32,34,35] Our measured I(D)/I(G) is consistent with that usually reported for the chemical vapor deposited (CVD) MWNTs used here.[36,37]

In the low frequency region, the Radial Breathing Modes (RBMs) are observed. Their position Pos(RBM), is inversely related to nanotube diameter ($d$) by Pos(RBM)=($C_1/d$)+$C_2$.[38] A variety of $C_1$ and $C_2$ were proposed for this relation.[38–42] Here we use the $C_1$=214.4cm$^{-1}$nm and $C_2$=18.7 cm$^{-1}$, from Ref. 38. These were derived by plotting the resonance energy as a function of inverse RBM frequency without any additional assumptions. Given the 36cm$^{-1}$ cut off frequency of our notch filter, according to the above relation, we are able to observe RBMs for tubes with diameter $<$12nm. Figure 2(b) shows that the tail of a broad RBM band is observed around $\sim$30-50cm$^{-1}$. This gives an estimate diameter distribution $\sim$7-10nm. This matches with the diameter distribution of the inner walls of the MWNTs we use here.[30]

Figure 2(a,b) indicate that the precursor nitrate salt mixtures Y123P and Y211P (prepared as

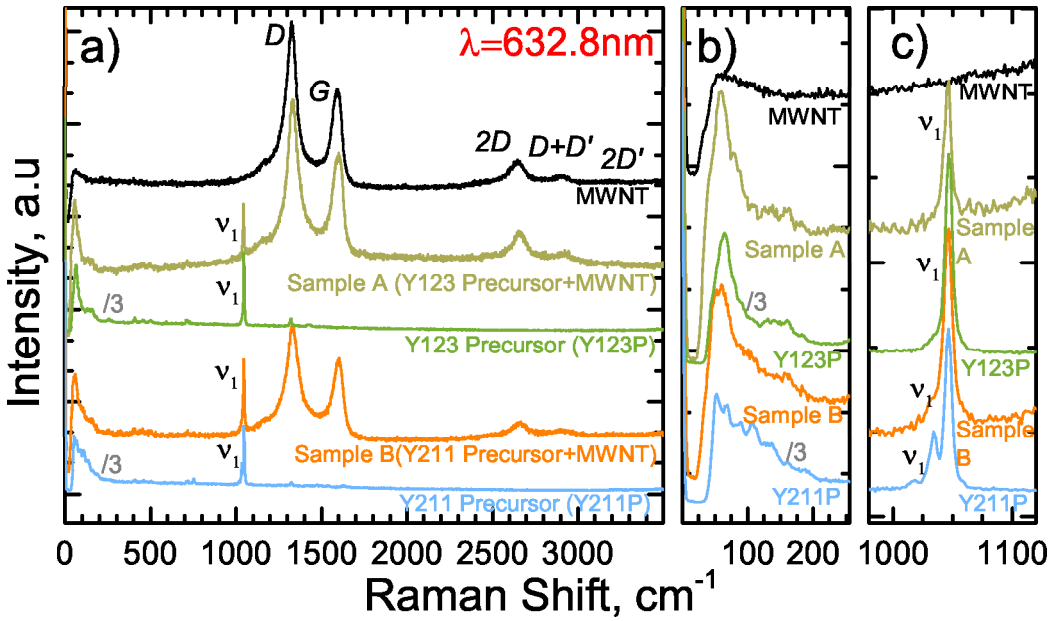


Figure 2: a) Raman spectra of MWNTs, Nitrate-MWNT dried precursor samples (A, B) and precursor nitrate salt mixtures (Y123P, Y211P). Expanded b) low frequency region from 0-250cm$^{-1}$ c) symmetric in-phase N-O stretching from the precursor nitrates in the 1000-1100cm$^{-1}$ region.

described in Methods) have Raman bands in the low frequency region. These are usually assigned to vibrations of water molecules[43] and nitrate ions.[43,44] We also observe a peak at$\sim$1045cm$^{-1}$, Figure 2(c), labeled $\nu_1$. We assign this to the symmetric, in-phase N-O stretching from $NO_3^-$ in $Ba(NO_3)_2$ and hydrated $Y(NO_3)_3$ precursor salts.[49–51] The low frequency component at $\sim$1034cm$^{-1}$ in sample Y211P is due to the higher cation molar fraction of hydrated $Y(NO_3)_3$ in the precursors.

The Raman spectra of Samples A and B, which contain Y-123 and Y-211 precursor salts in the same cation molar ratio as Y123P and Y211P in addition to MWNTs, show strong carbon signal, see Figure 2(a). The overall shape of the carbon-related Raman spectra is similar to that of the original MWNT powder. The low frequency bands in the mixtures are a signature of the the precursor salt, and overshadow any possible RBM. We also observe the $\nu_1$ peak$\sim$1045cm$^{-1}$ from the hydrated nitrate salts.

We then measure Samples A2 (Y-123) and B2 (Y-211) and their commercial counterparts, Figure 3. We do not detect any D or G peaks. We thus conclude that the MWNTs have been completely decomposed during the repeated high-temperature calcination in air. Sample A2 shows peaks in

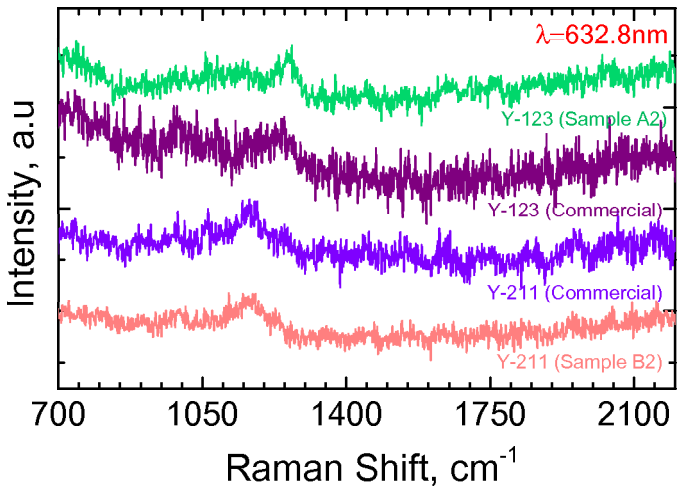


Figure 3: Raman spectra of samples A2 and B2 and their commercial Y-123 and Y-211 counterparts at 632.8nm excitation.

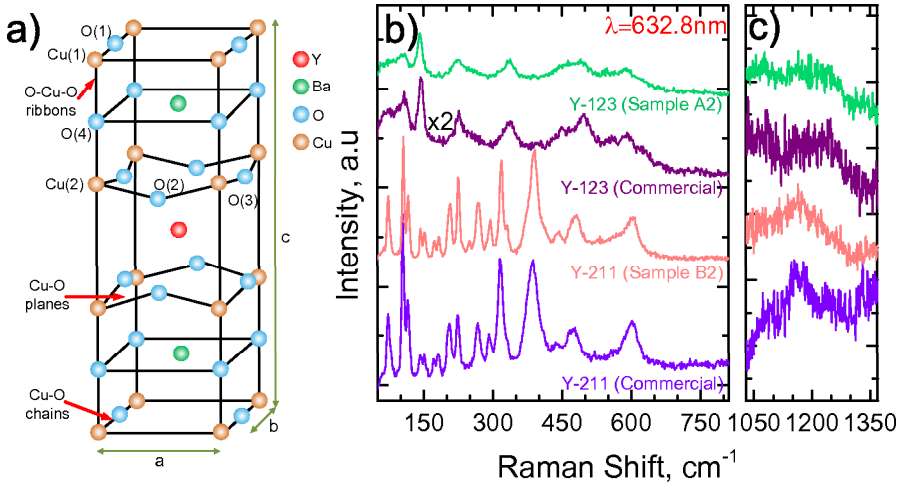


Figure 4: a) Orthorhombic unit cell of Y-123 b,c) Raman spectra of samples A2 and B2 compared to commercial Y-123 and Y-211 powders measured at 632.8nm

the$\sim$350-600 $cm^{-1}$ region, see Figure 4(b). In general, for YBCO, the modes above$\sim$300$cm^{-1}$ are related to oxygen.[52] The unit cell of Y-123 (Figure 4(a)) consists of basal Cu planes partially filled with O atoms and separated from the $CuO_2$ planes (Cu2-O2,O3) by BaO (Ba-O4) planes, see Ref. 53. The Raman peaks$\sim$335-440$cm^{-1}$ are usually assigned to out-of- and in-phase vibrations of these O2-O3 oxygen atoms with the $CuO_2$ planes.[54,55] The peak$\sim$490-500 $cm^{-1}$ is assigned to the vibration of oxygen O4 in apical sites of the orthorhombic phase of Y-123.[54–56] Sample A2 therefore exhibits peaks characteristic of Y-123,[55,57,58] as seen from the comparison with the commercial Toshima Y-123 powder in Figure 4(b). The bands$\sim$585-640$cm^{-1}$ are assigned to oxygen atom vibrations in the O-Cu-O ribbons(see Figure 4(a)).[59]

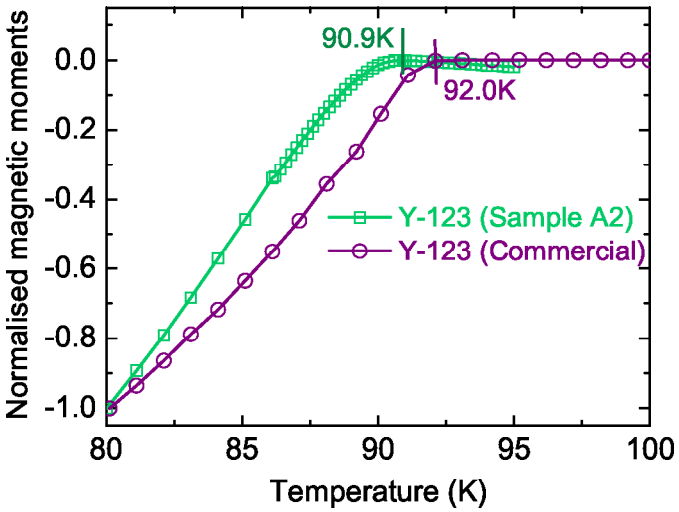


Figure 5: Comparison of $T_c$ of commercial Y-123 powder with that of Y-123 powder (sample A2) fabricated from the CNT templates.

The peaks in Sample B2 are also comparable to commercial Toshima Y-211.[52,60] A detailed assignment can be found in Ref. 52. In summary, the peaks$\sim$317, $\sim$390, $\sim$477$cm^{-1}$ are due to vibration of O2, O3 oxygen atoms,[52] and that$\sim$600$cm^{-1}$ is due to vibration modes of O3 oxygen atoms in Y-211.[52,60] The peak$\sim$1169$cm^{-1}$ in Figure 4(c) was assigned to low energy electronic excitations of Cu(II) in Y-211.[60,61]

To further study the purity of the superconducting phase, we measure $T_c$ of sample A2 and compare it to Toshima Y-123, Figure 5 (see Methods for measurements details). A2 shows superconducting behavior with an onset $T_c$=90.9K, comparable to Toshima Y-123. This indicates that

the use of CNTs as templates to fabricate nano-structured Y-123 does not affect $T_c$.

The lattice structure of the Y-123 and Y-211 nanopowders (A2 and B2) is determined using a D500/501 X-Ray diffractometer; see Figure 6(a,b). XRD patterns of commercial Toshima powders are also measured. The XRD peaks in A2 and B2 coincide with the commercial powders. This demonstrates that the CNT template does not affect the lattice structure of the final powder. XRD further confirms that the mixture of the nitrates of Y, Ba and Cu decomposes to form stoichiometric Y-123 and Y-211 in the presence of CNTs. We see a small amount of Y-211 in the XRD pattern of A2. Note that, to balance the overall chemical composition, an appropriate amount of $Ba_3Cu_5O_8$ should be present in this sample. As the main peaks of $Ba_3Cu_5O_8$ overlap with those of Y-123 and Y-211, it is not easy to identify the exact quantity. However a trace of Y-211 and $Ba_3Cu_5O_8$ in the final powder is not significant with regards to the development of YBCO superconductors, since the two phases are mixed and react peritectically to form Y-123 during melt-processing.[4] Further, the amount of Y-211 and $Ba_3Cu_5O_8$ can be reduced by calcining A2 repeatedly at 880°C, or slightly higher (e.g.$\sim$900 °C).

To determine their respective dimensions and distributions, the ground, calcined powders (A2, B2) are next examined by transmission electron microscopy (TEM) (see Methods). Drops of A2 and B2 liquid dispersions prepared by mixing the powders with water are dispensed on Holey carbon grids. We use a Tecnai T20 high resolution TEM with an acceleration voltage of 200KV in energy filtered mode. The particles have different morphologies and sizes, ranging from 4 to 100nm, with some agglomerates as large as 500nm, especially in B2. The statistical analysis on the powders is based on inspection of over 40 TEM images. Figure 7(a) shows the particle size distribution for Y-123 (A2) and Y-211 (B2). We find that A2, on average, consists of 12nm particles, whereas 30% of the particles in B2 are$>$75nm. The remainder 70% particles in B2 have an average size$\sim$30nm.

The particle size in B2 is also examined in the melt-processed single grain sample, Figure 8(a), fabricated using B2 with commercial Y-123 as matrix. Figure 8(b) compares the microstructure of this sample with a YBCO single grain containing commercial Y-211 and Y-123. Normally,

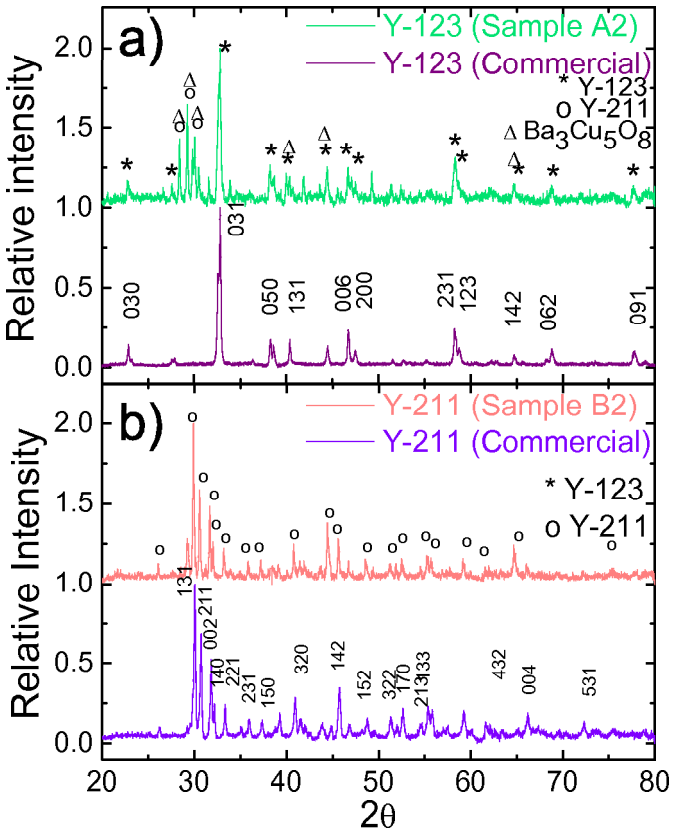


Figure 6: XRD patterns of a) sample A2 (Y-123) and b) sample B2 (Y-211) compared with commercial Toshima powders.

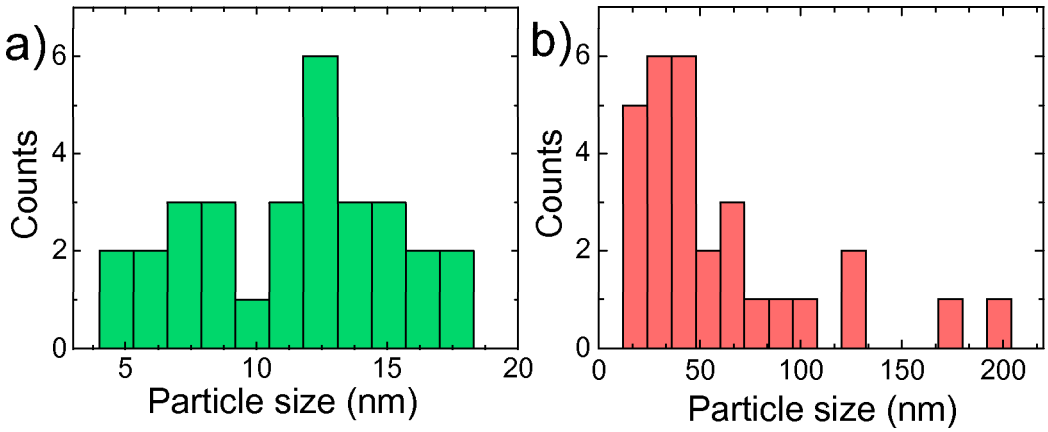


Figure 7: Particle size distribution for a) sample A2 (Y-123) and b) sample B2 (Y-211)

superconducting YBCO single grains contain a Y-123 phase matrix with Y-211 particles as inclusions.[4,11,12,62] The Y-211 particle size during melt-processing typically increases to between 1 and 5$\mu$m at high temperature (i.e. 1000°C for>100hrs).[63] The comparison between Figure 8(a) and (b) confirms that the particle size of sample B2 remains less than 1$\mu$m. This is due to the nanometer dimensions of the starting B2 powder.

For type II HTS, $J_c$ can be determined from:[64]

$$J_c = \frac{N\,\mu_o\,H_c^2\,\pi\,\xi\,d}{2B} \tag{1}$$

where $\mu_o$ is the permeability of free space, N is the number of pinning centres in a unit volume, $H_c$ is the critical magnetic field, $\xi$ is the coherence length, d is the size of the non-superconducting inclusion (i.e. pinning centre) and B is the magnetic field. Increasing the number of pinning centres in a given volume is necessary to increase $J_c$.[11,15] We observe smaller particles of Y-211 in Figure 8(a) compared to Figure 8(b). Thus, there will be more pinning centres in the YBCO single grain prepared from sample B2 compared to that prepared from commercial Toshima Y-211. Therefore we expect the former sample to exhibit higher $J_c$ and trapped field.

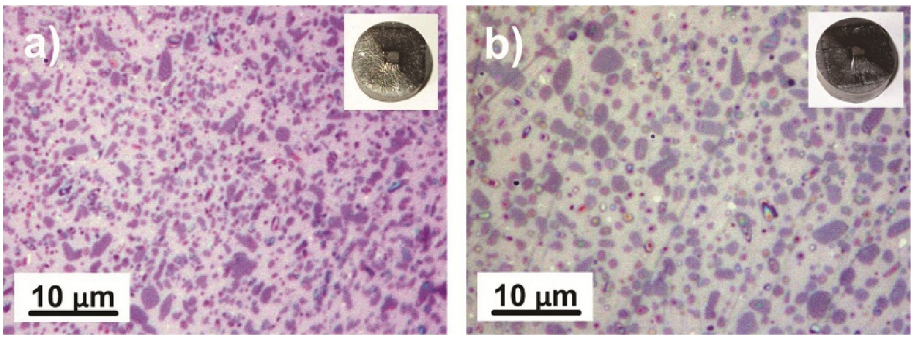


Figure 8: Microstructure comparison of YBCO single grain samples using fabricated using Y-211 (sample B2) a) and commercial Y-211 (Toshima) b)

In general, for single grain samples fabricated via TSMG, $J_c$ varies across the sample.[65,66] For example, $J_c$ is usually the lowest directly under the seed,[65,66] and gradually increases away from it.[66] The schematic in Figure 9(a) shows the four specimen positions that we use to measure $J_c$ relative to the seed, cut from the slice (shown in light green) taken from the single grain. The axes

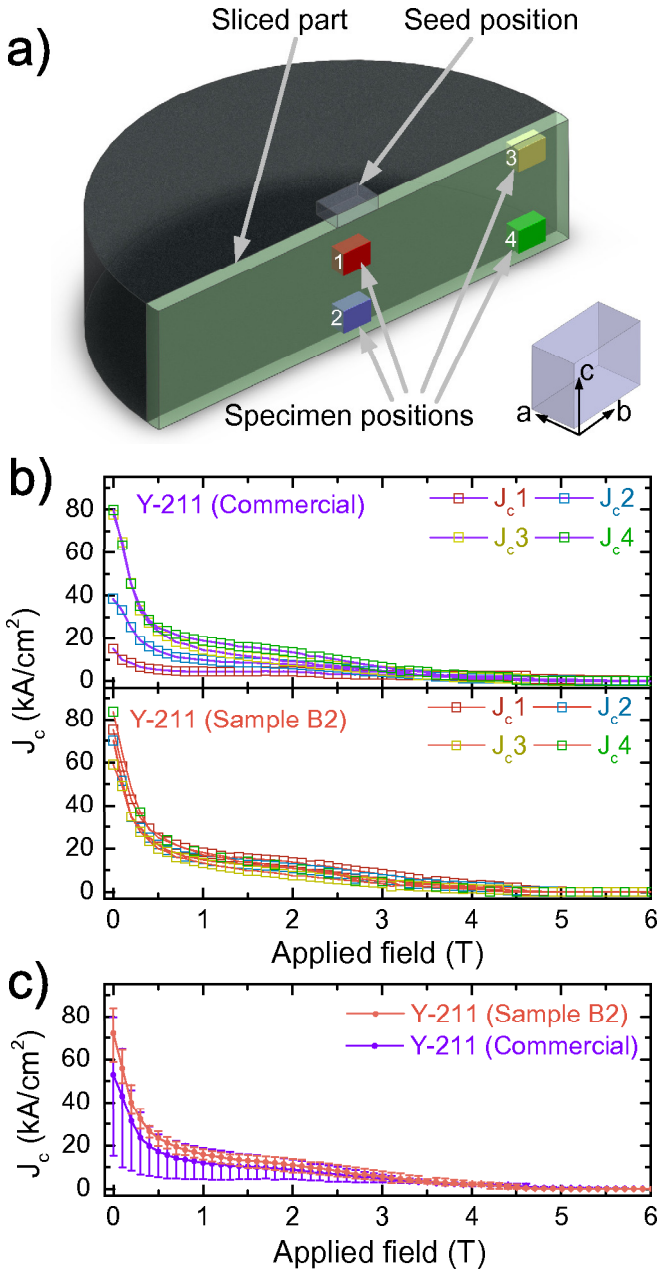


Figure 9: a) Schematic of the specimens cut from the single grain sample, in order to study the spatial variation of the superconducting properties. A ∼1 mm slice (light green) is taken from the middle of the grain, and then specimens are cut from this in four selected locations relative to the seed position. b) Measured $J_c$ of the samples fabricated using Y-211 (B2) and commercial Y-211 for the four different specimens, as indicated in a). c) Comparison of average $J_c$. The bars indicate the maximum and minimum measured values.

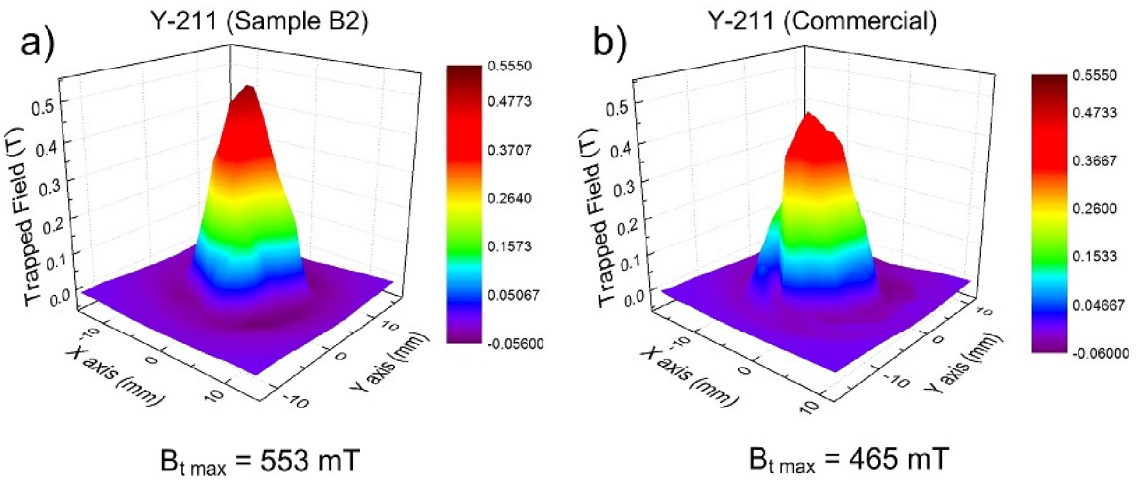


Figure 10: Comparison of the trapped field of the single grain fabricated from Y-211 (sample B2) and Y-211 (Toshima).

relative to the sample orientation are also shown. The color-coded plot in Figure 9(b) compares $J_c$ of the four colored specimens measured in single grain samples fabricated from Y-211 (Toshima) and Y-211(B2). The $J_c$ values in Y-211(B2) are very uniform compared to commercial Y-211. This indicates a uniform distribution of pinning centres. Figure 9(c) plots the average $J_c$ from the same four pieces as Figure 9(a,b). The highest and lowest $J_c$ at each point are also shown. We observe a$\sim$20% improvement in average $J_c$ at zero field compared to the sample prepared from commercial Y-211. This improvement is of significant importance for a range of applications,[2] as higher $J_c$ supports superconductivity with stronger fields.

Bulk HTS can potentially sustain considerably higher magnetic (trapped) fields than conventional permanent magnets.[2,4,67] The trapped field is proportional to $J_c$ and the volume of the superconductor.[2,12,68] It is more difficult to achieve a higher trapped field compared to higher $J_c$ because of the presence of large voids and cracks in the bulk sample[2] which block the super-current. As shown in Figure 10(a), we record 553mT trapped field for the single grain 16mm sample. This is$\sim$20% higher than the sample containing Toshima Y-211 (see Figure 10(b)) and is comparable to that usually obtained from similar samples with 20-25mm diameter[69] for the same experimental conditions. However, smaller samples are easier to fabricate due to the lower furnace requirements and shorter time of melt-processing. Also, from the application point of view, the bulk supercon-

ductor fabricated using sample B2 with its higher trapped field, can replace larger samples, e.g. in superconducting bearings,[2] reducing the overall cost and size of implementations.

# Conclusions

We demonstrated a fabricating process to produce nano-sized non-superconducting Y-211 and superconducting Y-123 powders using CNTs as templates. The resulting average particle size is$\sim$12 and $\sim$30nm, respectively. The use of CNTs does not affect either the superconducting transition temperature or the lattice structure. We recorded a trapped field 553mT for a 16mm diameter sample containing nano size Y-211 and commercial Y-123 with $\sim$20% improvement in average $J_c$ at 0 field compared to a sample containing commercial Y-211 and Y-123. Our method is general, and can be used to fabricate other nano-size powders, such as Y-2411(M).[8,10]

# Methods

## Preparation of nitrate solutions of Y-123 and Y-211

$Y(NO_3)_3$ (Alfa, 99.9% purity), $Ba(NO_3)_2$ (Alfa, 99.9%) and $Cu(NO_3)_2$ (Alfa, 99.9%) precursor powders are weighed in the appropriate cation molar ratios to form the $YBa_2Cu_3O_{6.5}$ and $Y_2BaCuO_5$ phases, respectively, according to the following empirical equations. Note that the final oxygen content in the non-stoichiometric samples may vary according to the fabrication method.

$$Y(NO_3)_3 + 2Ba(NO_3)_2 + 3Cu(NO_3)_2 \rightarrow YBa_2Cu_3O_{6.5}$$

$$2Y(NO_3)_3 + Ba(NO_3)_2 + Cu(NO_3)_2 \rightarrow Y_2BaCuO_5$$

The nitrate powders are dissolved in distilled water at room temperature to yield a final$\sim$0.6mol/litre concentration of Y-123 and Y-211. As a reference, an aliquot of the Y-123 and Y-211 solutions is dried without the MWNTs: Samples Y123P and Y211P, respectively.

## Dispersion of CNTs

We use MWNTs with ∼10-20 nm outer diameter and 5-10 nm inner diameter(Sigma-Aldrich, 636525).[30] 8mg MWNTs are dispersed in 20ml deionized (DI) water by ultrasonication for 40 minutes (Branson, 450A, 20-25°C). The resulting dispersions are then centrifuged using a MLA-130 fixed-angle rotor (Beckman) for 2 hours at a *g*-force of 1500-2000*g* (where *g* denotes the acceleration due to gravity). The super-natants, free from large MWNT bundles and other carbonaceous impurities, are then decanted from the centrifuge tube.

## Fabrication of superconducting powders using CNT as template

The CNT dispersion is mixed with the $YBa_2Cu_3O_{6.5}$ and $Y_2BaCuO_5$ based nitrate solution (1:4 vol%) using tip ultrasonication (Hielscher) for 10 minutes at 40W output power. This is then dried in air for 4 days, then calcined in an Ar atmosphere at 600°C for 10 hours to eliminate the nitrates. Finally, the powders are calcined repeatedly (three times) at 880°C for 10 hours in air to eliminate carbon from and form the target Y-123 and Y-211 phases.

## Fabrication of superconducting single grain using nano-structured Y-211 (B2)

Superconducting YBCO single grains are fabricated via TSMG.[12] Powders of Y-123 (99.9% Toshima), Y-211 (sample B2) and Pt (to inhibit coarsening of the Y-211 particle size during melt-processing at high temperature[7]) are mixed in a composition of (70 wt% Y-123 + 30 wt% Y-211) + 0.1 wt%Pt. 10g of mixed powder is then pressed uniaxially into a pellet of diameter 20mm. A NdBCO seed is placed on the top surface of the pellet at room temperature to promote heterogeneous nucleation during melt processing. The sample is then heated to 1045°C for 1.0 hour, cooled to 1015°C at a rate of 120°C/h, then slow cooled to 975°C at 0.4°C/h, and furnace cooled to room temperature. As a result, the diameter shrinks to 16mm. The sample is then polished using a diamond spray and its microstructure analyzed using a Nikon ECLIPSE ME600 optical microscope. Finally, the particle size of Y-211 is compared with that of a standard sample fabricated

using commercially available Y-211(Toshima).

## Measurements of $T_c$, $J_c$ and Trapped field

$T_c$ is measured under zero field cooled condition (i.e. cooled to a temperature which is lower than $T_c$ before a field is applied[2]) with an applied field of 10Oe, using a superconducting quantum interface device (SQUID). For the trapped field measurements, the top surfaces of the samples are polished flat. The trapped magnetic field profiles at the samples' top surfaces are measured using a home made Hall probe flux-scanning system. Samples are then field cooled, followed by the application of 0.8T. The Hall probes (20 probes in a line) of the system are positioned 0.5mm above the sample surface and rotated 360 degrees during the measurements. Then the single grain samples are sliced from middle as shown in Figure 9. The slices are further cut into smaller pieces for $J_c$ measurements. The size of the specimens are $\sim 1.5 \times 1.5 \times 1.0 mm^3$. From the magnetic moments obtained from a SQUID, an extended Bean model is employed to calculate $J_c$ ($A/cm^2$) at 77 K using the relation:[70]

$$J_c = \frac{20\Delta m\, a\left(1 - \frac{a}{3b}\right)}{abc}$$

where $\Delta m$ (emu) represents the difference in magnetic moment observed in the M-H loops for increasing and decreasing field cycles with the applied field perpendicular to the *ab* plane and a, b and c are the dimensions (cm) of the sample with a<b.

## Acknowledgement

YS thanks funding from EPSRC (EP/H049657/1), TH from King's College, Cambridge, and the Royal Academy of Engineering, ACF from ERC grant NANOPOTS and Royal Society Wolfson Research Merit Award.

## References


1. Shiohara, Y.; Endo, A., Crystal growth of bulk high-Tc superconducting oxide materials *Mater. Sci. Eng., R.* **19**, 1-86 (1997)

2. Krabbes, G., Fuchs, G., Canders, W.-R., May, H. and Palka, R., High Temperature Superconductor Bulk Materials, (Wiley-VCH Verlag GmbH & Co. KGaA, Weinheim, 2006).

3. Campbell, A. M., Factors limiting current densities in oxide superconductors *Physica B.* **216**, 266-268 (1996)

4. Murakami, M., *Melt-processed high-temperature superconductors*, World Scientific, 1992.

5. Umezawa, A.; Crabtree, G. W.; Liu, J. Z.; Weber, H. W.; Kwok, W. K.; Nunez, L. H.; Moran, T. J.; Sowers, C. H. and Claus, H., Enhanced critical magnetization currents due to fast neutron irradiation in single-crystal $YBa_2Cu_3O_{7-x}$. *Physical Review B* **36**, 7151-7154 (1987)

6. Iida, K.; Nadendla, H. Babu,; Reddy, E.S.; Shi, Y and Cardwell D. A., The effect of nano-size $ZrO_2$ powder addition on the microstructure and superconducting properties of single-domain Y-Ba-Cu-O bulk superconductors *Supercond. Sci. Technol.* **18**, 249-254, (2005)

7. Izumi, T.; Nakamura, Y.; Shiohara, Y., Doping effects on coarsening of $Y_2BaCuO_5$ phase in liquid *J. Mater. Res.* **8**, 1240-1246 (1993)

8. Babu, N. H.; Reddy, E. S.; Cardwell, D. A.; Campbell, A. M.; Tarrant, C. D.; Schneider, K. R., Artificial flux pinning centers in large, single-grain (RE)-Ba-Cu-O superconductors *Appl. Phys. Lett.* **83**, 4806-4808 (2003)

9. Kumar, P.; Pillai, V.; Bates, S. R.; Shah, D. O., Preparation of $YBa_2Cu_3O_{7-x}$ superconductor by coprecipitation of nanosize oxalate precursor powder in microemulsions *Mater. Lett.* **16**, 68-74 (1993)

10. Pathak, S. K.; Yeoh, W. K.; Babu, N. H.; Shi, Y.; Iida, K.; Strasik, M.; Cardwell, D. A., Fabrication of high performance Y-123/Y-24Nb1/Ag single grain composites *Physica C: Superconductivity.* **469**, 1173-1177 (2009)

11. Lo, W.; Cardwell, D. A.; Dewhurst, C. D.; Dung, S.-L., Fabrication of large grain YBCO by seeded peritectic solidification *Journal of Materials Research.* **11**, 786-794 (1996)

12. Cardwell, D. A., Processing and properties of large grain (RE)BCO *Materials Science and Engineering: B.* **53**, 1-10 (1998)

13. Griffith, M. L.; Huffman, R. T.; Halloran, J. W., Formation and Coarsening Behavior of Y2BaCuO5 from Peritectic Decomposition of $YBa_2Cu_3O_{7-X}$ *Journal of Materials Research.* **9**, 1633-1643 (1994)

14. Sawano, K.; Morita, M.; Tanaka, M.; Sasaki, T.; Kimura, K.; Takebayashi, S.; Kimura, M.; Miyamoto, K., High Magnetic Flux Trapping by Melt-Grown YBaCuO Superconductors *Japanese Journal of Applied Physics.* **30**, L1157

15. Murakami, M., Processing of bulk YBaCuO *Superconductor Science and Technology.* **5**, 185 (1992)

16. Website URL: http://www.material-sys.com/en/product/, accessed on May 31, 2011

17. Zhou, L.; Chen, S. K.; Wang, K. G.; Wu, X. Z.; Zhang, P. X.; Feng, Y., Synthesis of ultrafine $Y_2BaCuO_5$ powder and its incorporation into YBCO bulk by powder melting process *Physica C: Superconductivity.* **363**, 99-106 (2001)

18. Bhargava, A.; Alarco, J.; Mackinnon, I. D. R.; Yamashita, T., Manufacture of fine grained $Y_2BaCuO_5$ powder by co-precipitation *Materials Letters.* **24**, 181-188 (1995)

19. Lo, W.; Cardwell, D. A.; Shi, Y. H., Spray dried Pt-doped Nd-Ba-Cu-O precursor powder for seeded peritectic processing of large superconducting grains *Mater. Sci. Eng., B.* **65**, 1-10 (1999)

20. Li, F.; Vipulanandan, C.; Zhou, Y. X.; Salama, K., Nanoscale $Y_2BaCuO_5$ particles for producing melt-textured YBCO large grains *Supercond. Sci. Technol.* **19**, 589 (2006)

21. Kumar, N. D.; Rajasekharan, T.; Muraleedharan, K.; Banerjee, A.; Seshubai, V., Unprecedented current density to high fields in $YBa_2Cu_3O_{7-d}$ superconductor through nano-defects generated by preform optimization in infiltration growth process *Superconductor Science and Technology.* **23**, 105020 (2010)

22. Li, F.; Vipulanandan, C., Characterization of $Y_2BaCuO_5$ nanoparticles synthesized by nano-emulsion method *Journal of Nanoparticle Research.* **9**, 841-852 (2007)

23. Chikkannanavar, S. B.; Smith, B. W.; Luzzi, D. E. in Carbon Nanotubes: Properties and Applications, *Eds: OConnell, M. J.* CRC Press,Boca Raton, FL (2006)

24. Ajayan, P. M.; Stephan, O.; Redlich, P.; Colliex, C., Carbon nanotubes as removable templates for oxide nanocomposites and nanostructures *Nature.* **375**, 564-567 (1995)

25. Sun, Z.; Zhang, H.; Zhao, Y.; Huang, C.; Tao, R.; Liu, Z.; Wu, Z., Thermal-Stable Carbon Nanotube-Supported Metal Nanocatalysts by Mesoporous Silica Coating *Langmuir.* **27**, 6244-6251 (2011)

26. Whitby, R. L. D.; Hsu, W. K.; Boothroyd, C. B.; Brigatti, K. S.; Kroto, H. W.; Walton, D. R. M., $WS_2$ layer formation on multi-walled carbon nanotubes *Applied Physics A: Materials Science & Processing.* **76**, 527-532 (2003)

27. Shi, Y.; Hari Babu, N.; Iida, K.; Cardwell, D. A., Mg-doped Nd-Ba-Cu-O generic seed crystals for the top-seeded melt growth of large-grain (rare earth)-Ba-Cu-O bulk superconductors. *Journal of Materials Research.* **21**, 1355-1362 (2006)

28. Hasan, T.; Scardaci, V.; Tan, P. H.; Rozhin, A. G.; Milne, W. I.; Ferrari, A. C., Stabilization and de-bundling of single-wall carbon nanotube dispersions in N-Methyl-2-Pyrrolidone (NMP) by polyvinylpyrrolidone (PVP) *J. Phys. Chem. C.* **111**, 12594-12602 (2007)

29. Hasan, T.; Sun, Z.; Wang, F.; Bonaccorso, F.; Tan, P. H.; Rozhin, A. G.; Ferrari, A. C., Nanotube-Polymer Composites for Ultrafast Photonics *Adv. Mater.* **21**, 3874-3899 (2009)

30. Website URL: http://www.sigmaaldrich.com/catalog/ProductDetail.do?D7=0&N5=SEARCH_CONCAT_PNO|BRAND_KEY&N4=636525|ALDRICH&N25=0&QS=ON&F=SPEC, accessed on October 21, 2011

31. Sofie, S. W.; Dogan, F., Effect of carbon on the microstructure and superconducting properties of YBa2Cu3$O_{7-x}$ melt-textured crystals *Supercond. Sci. Technol.* **15**, 735 (2002)

32. Ferrari, A. C.; Robertson, J., Interpretation of Raman spectra of disordered and amorphous carbon *Phys. Rev. B.* **61**, 14095-14107 (2000)

33. Piscanec, S.; Lazzeri, M.; Robertson, J.; Ferrari, A. C.; Mauri, F., Optical phonons in carbon nanotubes: Kohn anomalies, Peierls distortions, and dynamic effects *Phys. Rev. B.* **75**, 035427 (2007)

34. Ferrari, A. C., Raman spectroscopy of graphene and graphite: Disorder, electron-phonon coupling, doping and nonadiabatic effects *Solid State Commun.* **143**, 47-57 (2007)

35. Cancado, L. G.; Jorio, A.; Ferreira, E. H. M.; Stavale, F.; Achete, C. A.; Capaz, R. B.; Moutinho, M. V. O.; Lombardo, A.; Kulmala, T. S.; Ferrari, A. C., Quantifying Defects in Graphene via Raman Spectroscopy at Different Excitation Energies *Nano Lett.* **11**, 3190-3196 (2011)

36. Chhowalla, M.; Teo, K.; Ducati, C.; Rupesinghe, N.; Amaratunga, G.; Ferrari, A.; Roy, D.; Robertson, J.; Milne, W., Growth process conditions of vertically aligned carbon nanotubes using plasma enhanced chemical vapor deposition *J. Appl. Phys.* **90**, 5308 (2001)

37. Tan, P.; Zhang, S.-L.; Yue, K. T.; Huang, F.; Shi, Z.; Zhou, X.; Gu, Z., Comparative Raman Study of Carbon Nanotubes Prepared by D.C. Arc Discharge and Catalytic Methods *J. Raman Spectrosc.* **28**, 369-372 (1997)

38. Telg, H.; Maultzsch, J.; Reich, S.; Hennrich, F.; Thomsen, C., Chirality Distribution and Transition Energies of Carbon Nanotubes *Phys. Rev. Lett.* **93**, 177401 (2004)

39. Rao, A. M.; Richter, E.; Bandow, S.; Chase, B.; Eklund, P. C.; Williams, K. A.; Fang, S.; Subbaswamy, K. R.; Menon, M.; Thess, A.; Smalley, R. E.; Dresselhaus, G.; Dresselhaus, M. S., Diameter-selective Raman scattering from vibrational modes in carbon nanotubes *Science.*, **275**, 187-191 (1997)

40. Meyer, J. C.; Paillet, M.; Michel, T.; Moreac, A.; Neumann, A.; Duesberg, G. S.; Roth, S.; Sauvajol, J. L., Raman modes of index-identified freestanding single-walled carbon nanotubes *Phys. Rev. Lett.* **95**, 217401 (2005)

41. Jorio, A.; Saito, R.; Hafner, J. H.; Lieber, C. M.; Hunter, M.; McClure, T.; Dresselhaus, G.; Dresselhaus, M. S., Structural (n, m) determination of isolated single-wall carbon nanotubes by resonant Raman scattering *Phys. Rev. Lett.* **86**, 1118-1121 (2001)

42. Araujo, P. T.; Doorn, S. K.; Kilina, S.; Tretiak, S.; Einarsson, E.; Maruyama, S.; Chacham, H.; Pimenta, M. A.; Jorio, A., Third and fourth optical transitions in semiconducting carbon nanotubes *Phys. Rev. Lett.* **98**, 067401 (2007)

43. Kanno, H; Hiraishi, J., Raman study of aqueous rare earth nitrate solutions in liquid and glassy states *J. Phys. Chem.* **88**, 2787-2792 (1984)

44. Guofa, L., Tongshun, S. and Yongnian, Z., Journal of Molecular Structure, **412**, 75-81 (1997).

45. Chen, G.; Bandow, S.; Margine, E. R.; Nisoli, C.; Kolmogorov, A. N.; Crespi, V. H.; Gupta, R.; Sumanasekera, G. U.; Iijima, S.; Eklund, P. C., Chemically Doped Double-Walled Carbon Nanotubes: Cylindrical Molecular Capacitors *Phys. Rev. Lett.* **90**, 257403 (2003)

46. Casiraghi, C.; Pisana, S.; Novoselov, K. S.; Geim, A. K.; Ferrari, A. C., Raman fingerprint of charged impurities in graphene *Appl. Phys. Lett.* **91**, 233108-3 (2007)

47. Pisana, S.; Lazzeri, M.; Casiraghi, C.; Novoselov, K. S.; Geim, A. K.; Ferrari, A. C.; Mauri, F., Breakdown of the adiabatic Born-Oppenheimer approximation in graphene *Nat Mater* **6**, 198-201 (2007)

48. Zhao, W., Tan, P. H., Liu, J. and Ferrari, A. C., Journal of the American Chemical Society, **133**, 5941-5946 (2011)

49. Mathieu, J.-P.; Lounsbury, M., The Raman spectra of metallic nitrates and the structure of concentrated solutions of electrolytes *Discussions of the Faraday Society.* **9**, 196-207 (1950)

50. Waterland, M., Symmetry breaking effects in $NO_3$: Raman spectra of nitrate salts and ab initio resonance Raman spectra of nitrate-water complexes *Journal of Chemical Physics.* **114**, 6249 (2001)

51. Waterland, M., Far-ultraviolet resonance Raman spectroscopy of nitrate ion in solution *Journal of Chemical Physics.* **113**, 6760 (2000)

52. Abrashev, M. V.; Iliev, M. N., Polarized Raman spectra of $Y_2BaCuO_5$: Normal-mode assignment from substitutions for Y and Ba *Physical Review B.* **45**, 8046 (1992)

53. Faulques, E., in Book *Materials Synthesis and Characteriztion*, Perry, Dale L., Eds.; Plenum Press, New York, 1997

54. Thomsen, C.; Litvinchuk, A. P.; Schonherr, E.; Cardona, M., *Physical Review B.* **45**, 8154-8157 (1992)

55. Camerlingo, C.; Delfino, I.; Lepore, M., Micro-Raman spectroscopy on YBCO films during heat treatment *Superconductor Science and Technology.* **15**, 1606 (2002)

56. Huong, P. V., Microstructure of high temperature superconductor thin films as studied by micro-Raman spectroscopy *Physica C: Superconductivity.* **180**, 128-131 (1991)

57. Barboy, I.; Camerlingo, C.; Bar, I.; Bareli, G.; Jung, G., Micro-Raman spectroscopy of laser processed $YBa_2Cu_3O_{7-d}$ thin films *Journal of Applied Physics.* **110**, 033912 (2011)

58. Palles, D.; Poulakis, N.; Liarokapis, E.; Conder, K.; Kaldis, E.; Muller, K. A., Raman study of the oxygen anharmonicity in $YBa_2Cu_3O_x$ ($6.4<x<7.0$) superconductors *Physical Review B.* **54**, 6721 (1996)

59. Burns, G.; Dacol, F. H.; Feild, C.; Holtzberg, F., Raman measurements of $YBa_2Cu_3O_x$ as a function of oxygen content *Solid State Communications.* **77**, 367-371 (1991)

60. Flavell, W. R.; Egdell, R. G., Observation of electronic Raman scattering in $Y_2BaCuO_5$ *Solid State Communications.* **69**, 631-633 (1989)

61. Udagawa, M.; Ogita, N.; Fukumoto, A.; Utsunomiya, Y.; Ohbayashi, K., Raman and Infrared Spectra of a Green $Y_2BaCuO_{5-y}$ *Jpn. J. Appl. Phys.* **26**, L858 (1987)

62. Shi, Y. H.; Yoeh, W.; Dennis, A. R.; Hari Babu, N.; Pathak, P.; Xu, Z.; Cardwell, D. A., Growth rate of YBCO single grains containing Y-2411(M) *Journal of Physics: Conference Series.* **234**, 012039 (2010)

63. Yeoh, W. K.; Pathak, S. K.; Yunhua, S.; Dennis, A. R.; Cardwell, D. A.; Babu, N. H.; Strasik, M., Improved Flux Pinning in Y-Ba-Cu-O Superconductors Containing Niobium Oxide *Applied Superconductivity, IEEE Transactions on.* **19**, 2970-2973 (2009)

64. Campbell, A. M.; Evetts, J. E., Flux vortices and transport currents in type II superconductors *Advances in Physics.* **21**, 199 (1972)

65. Shi, Y.; Babu, N. H.; Cardwell, D. A., Properties of GdBCO bulk superconductors melt-processed in air using a Mg-doped Nd-Ba-Cu-O generic seed crystal *Superconductor Science and Technology.* **20**, 38 (2007)

66. Dewhurst, C. D.; Wai, L.; Cardwell, D. A., Distribution of critical current density in large $YBa_2Cu_3O_{7-\delta}$ grains fabricated using seeded peritectic solidification *Applied Superconductivity, IEEE Transactions on.* **7**, 1925-1928 (1997)

67. Cardwell, D. A.; Hari Babu, N., Processing and properties of single grain (RE)-Ba-Cu-O bulk superconductors *Physica C: Superconductivity.* **445-448**, 1-7 (2006)

68. Tomita, M.; Murakami, M., High-temperature superconductor bulk magnets that can trap magnetic fields of over 17 tesla at 29K *Nature.* **421**, 517-520 (2003)

69. Xu, C.; Hu, A.; Sakai, N.; Izumi, M.; Hirabayashi, I., Effect of $Gd_2Ba_4CuMoO_y$ addition on the band structure and spatial variation of superconducting properties in $GdBa_2Cu_3O_{7-\delta}$ single domains *Superconductor Science and Technology.* **18**, 1082 (2005)

70. Bean, C. P., Magnetization of High-Field Superconductors *Reviews of Modern Physics.* **36**, 31 (1964)